Exploration Geophysics (2006) 37, 86-92
Butsuri-Tansa (Vol. 59, No. 1)
Mulli-Tamsa (Vol. 9, No. 1)

Improved full-waveform inversion of normalised seismic wavefield data

Hee Joon Kim[1] Toshifumi Matsuoka[2]

Key Words: crosshole, full waveform, tomography, normalised wavefield, sensitivities

ABSTRACT

The full-waveform inversion algorithm using normalised seismic wavefields can avoid potential inversion errors due to source estimation required in conventional full-waveform inversion methods. In this paper, we have modified the inversion scheme to install a weighted smoothness constraint for better resolution, and to implement a staged approach using normalised wavefields in order of increasing frequency instead of inverting all frequency components simultaneously. The newly developed scheme is verified by using a simple two-dimensional fault model. One of the most significant improvements is based on introducing weights in model parameters, which can be derived from integrated sensitivities. The model-parameter weighting matrix is effective in selectively relaxing the smoothness constraint and in reducing artefacts in the reconstructed image. Simultaneous multiple-frequency inversion can almost be replicated by multiple single-frequency inversions. In particular, consecutively ordered single-frequency inversion, in which lower frequencies are used first, is useful for computation efficiency.

INTRODUCTION

In crosshole seismic applications, typical approaches involve ray tomography (e.g., Peterson et al., 1985; Nolet, 1985; Humphreys and Clayton, 1988; Scales et al., 1988; Vasco, 1991) and more recently Fresnel volume tomography (e.g., Cerveny and Soares, 1992; Vasco et al., 1995). Traveltime tomographies using ray tracing require high-frequency approximation, with maximum resolution on the order of a wavelength (Sheng and Schuster, 2000). Because of the lack of resolution, however, the usefulness of ray tomography may be limited, if the objective is to better understand the petrophysical and hydrological properties of soils and rocks. Such understanding is important in characterising petroleum and geothermal reservoirs and in environmental applications of various scales.

An alternative to traveltime tomography is full-waveform inversion. Recent studies (e.g., Sen and Stoffa, 1991; Kormendi and Dietrich, 1991; Minkoff and Symes, 1997; Zhou et al., 1997; Plessix and Bork, 1998; Pratt, 1999; Pratt and Shipp, 1999) suggest that full-waveform inversion can provide improved resolution of velocity structures. Full-waveform analyses can be useful for investigating hydrological and petrophysical properties of the medium because waveforms are sensitive to material properties through which the wave propagates. There is, however, one major difficulty to overcome in full-waveform inversion. In field applications, the effective source waveform, the coupling between the source and the medium, and the coupling between the receivers and the medium, are not very well understood. The problem can be alleviated to some extent with a good velocity approximation (Pratt, 1999), but in general measured signals cannot be properly calibrated, rendering full-waveform inversion technically difficult to apply.

It is highly desirable to develop an inversion algorithm that is independent of knowledge of the source wavelet because of the uncertainties in determining the shape of the source waveform. Frazer et al. (1997) and Frazer and Sun (1998) suggested a new objective function for inversion of sonic waveforms with unknown source and receiver functions. Pratt (1999) and Pratt and Shipp (1999) showed a practical waveform inversion scheme in the frequency domain, reconstructing both the source signature and properties of the interwell medium. Recently, normalised wavefield data in the frequency domain were shown to be effective for source-independent full-waveform inversion (Zhou and Greenhalgh, 2003; Lee and Kim, 2003); Zhou and Greenhalgh (2003) used normalised Fourier amplitude data, while Lee and Kim (2003) employed normalised real- and imaginary-component data.

In the normalised wavefield approaches, seismic data are first transformed into the frequency domain and a set of normalised wavefields is constructed. Since the normalised wavefield is independent of the source spectrum, their methods allow full-waveform inversion without requiring the knowledge of source signature. In this paper, we further exploit the approach developed by Lee and Kim (2003), to install a weighted smoothness constraint into the inversion scheme for better resolution, and adopt a staged inversion approach, from low to high frequencies, instead of inverting all frequency information simultaneously. We test the staged multiple single-frequency inversion to reduce total inversion time.

NORMALISED WAVEFIELD

The source-independent full-waveform inversion algorithm using normalised wavefields was described in detail in Lee and Kim (2003). For completeness, their algorithm is briefly outlined here.

Let us consider a simple two-dimensional (2D) acoustic wave equation in the frequency domain,

$$\nabla^2 p(\mathbf{x},\mathbf{x}_s,\omega)+\frac{\omega^2}{v^2(\mathbf{x})}p(\mathbf{x},\mathbf{x}_s,\omega)+\delta(\mathbf{x}-\mathbf{x}_s)=0\ , \qquad (1)$$

where p is the impulse response of the scalar pressure wavefield, ω is the angular frequency, v is the velocity, and $(\mathbf{x}, \mathbf{x}_s)$ are the field and source positions in 2D. The source is an impulse source expressed as a 2D spatial delta function $\delta(\mathbf{x}\text{-}\mathbf{x}_s)$ located at $\mathbf{x}_s$. The source is also a delta function $\delta(t)$ at $t = 0$ in the time domain.

[1] *Department of Environmental Exploration Engineering, Pukyong National University, Busan 608-737, Korea*
Email: hejkim@pknu.ac.kr

[2] *Department of Civil and Earth Resource Engineering, Kyoto University, Kyoto 606-8501, Japan*

Manuscript received 19 July, 2005.
Revised manuscript received 11 September, 2005.

Let us assume a crosshole survey involving NS sources and NG receivers. Field data, in general, may be described as

$$D_{ji}(t) = R_j(t) * P_{ji}(t) * S_i(t), \quad j = 1, 2, \ldots, NG, \; i = 1, 2, \ldots, NS, \tag{2}$$

where * denotes convolution in time, $D_{ji}(t)$ is the pressure, $P_{ji}(t)$ is the impulse response, $R_j(t)$ and $S_i(t)$ are the receiver and source functions, respectively. The pressure $D_{ji}(t)$ is measured at the j-th receiver position due to a source $S_i(t)$ at the i-th source position. The source function includes the source-medium coupling, therefore being an effective source. The receiver function $R_j(t)$ includes the medium-receiver coupling as well, but is ignored in the following analysis.

If we take the Fourier Transform of equation (2), for which

$$FT\{(D, P, S)(t)\} \rightarrow (d, p, s)(\omega),$$

we have

$$d_{ji}(\omega) = p_{ji}(\omega) s_i(\omega), \tag{3}$$

where ω is the angular frequency equal to 2π times the temporal frequency f. Next, to define the normalised wavefield, we first select a reference receiver, say with $j = 1$. The normalised wavefield t_{ji} is defined in such a way that $t_{ji} = d_{ji} / d_{1i}$, $j = 2, 3, \ldots, NG$, and so has the property of generating data at the j-th receiver position when it is multiplied by data from the reference point. Using equation (3), we obtain

$$t_{ji}(\omega) = \frac{d_{ji}(\omega)}{d_{1i}(\omega)} = \frac{p_{ji}(\omega) s_i(\omega)}{p_{1i}(\omega) s_i(\omega)} = \frac{p_{ji}(\omega)}{p_{1i}(\omega)}. \tag{4}$$

Since the source spectrum cancels out itself, the normalised wavefield is the same as the normalised impulse response of the medium. In the normalised wavefield approach, the functional to be minimised is the misfit in the normalised wavefield, not in the pressure wavefield, and therefore the source function is not involved in the inversion process (Lee and Kim, 2003).

INVERSION SCHEME

The seismic inverse problem can be expressed as

$$\Delta\mathbf{d} = \mathbf{J}\Delta\mathbf{m}, \tag{5}$$

where $\Delta\mathbf{d}$ is the vector of differences between measured and modelled data (normalised wavefields), $\Delta\mathbf{m}$ is the vector of corrections to the initial model $\mathbf{m}_0$, and $\mathbf{J}$ is the Jacobian matrix (the matrix of partial derivatives of modelled responses with respect to model parameters). A common approach for model parameterisation is to divide a model into many blocks of unknown velocities.

As in most geophysical inverse problems, a roughness (the reciprocal of smoothness) term should be introduced to stabilise the inversion process of equation (5) (Tikhonov and Arsenin, 1977). For the smoothest inversion, our objective function to be minimised is

$$U = \left\|\mathbf{W}_d(\mathbf{J}\Delta\mathbf{m} - \Delta\mathbf{d})\right\|^2 + \lambda\left[\left\|\mathbf{W}_m\mathbf{L}(\mathbf{m}_0 + \Delta\mathbf{m})\right\|^2 + \varepsilon\left\|\Delta\mathbf{m}\right\|^2\right], \tag{6}$$

where $\|\bullet\|$ denotes the Euclidean norm, $\mathbf{W}_d$ and $\mathbf{W}_m$ are data and model weighting matrices, respectively, λ is a Lagrange multiplier, ε is a positive constant, and $\mathbf{L}$ is a finite-difference operator to quantify model roughness (e.g., Sasaki, 1989; deGroot-Hedlin and Constable, 1990).

In equation (6), the regularisation parameter λ controls the trade-off between data misfit and model roughness (Tikhonov and Arsenin, 1977; Parker, 1994). Larger values of λ result in smooth and stable solutions, at the expense of resolution. In contrast, as λ gets smaller, the inverse problem becomes closer to an ill-conditioned least-squares problem, resulting in an erratic model (e.g., Parker, 1980). An additional way to constrain the inverse solution is to introduce weights. The data-weighting matrix $\mathbf{W}_d$ usually contains information on the importance of one data point with respect to the others. In this way, for example, the data of better quality will have a larger weight than the data of poor quality. In the same way that we introduced the weights for data, we can also introduce weights for model parameters to selectively relax the smoothness constraint.

Minimisation of equation (6) produces a system of linear equations in the form of a normal equation

$$\begin{aligned}\left[\mathbf{J}^T\mathbf{W}_d^T\mathbf{W}_d\mathbf{J} + \lambda\left(\mathbf{L}^T\mathbf{W}_m^T\mathbf{W}_m\mathbf{L} + \varepsilon\mathbf{I}\right)\right]\Delta\mathbf{m} \\ = \mathbf{J}^T\mathbf{W}_d^T\mathbf{W}_d\Delta\mathbf{d} - \lambda\mathbf{L}^T\mathbf{W}_m^T\mathbf{W}_m\mathbf{L}\mathbf{m}_0\end{aligned}, \tag{7}$$

or in the form of an observation equation

$$\begin{bmatrix}\mathbf{W}_d\mathbf{J} \\ \sqrt{\lambda}\mathbf{W}_m\mathbf{L} \\ \sqrt{\lambda\varepsilon}\mathbf{I}\end{bmatrix}\{\Delta\mathbf{m}\} = \begin{Bmatrix}\mathbf{W}_d\Delta\mathbf{d} \\ -\sqrt{\lambda}\mathbf{W}_m\mathbf{L}\mathbf{m}_0 \\ \mathbf{0}\end{Bmatrix}, \tag{8}$$

where $\mathbf{I}$ denotes the identity matrix. The solution obtained from equation (8) is known to be more accurate than the solution obtained via equation (7) (e.g., Lines and Treitel, 1984). The vector $\Delta\mathbf{m}$ is added to the initial vector $\mathbf{m}_0$ to update the parameters. The procedure is repeated until the misfit between measured and modelled data is reduced to an acceptable level. The rms misfit E_d is given by

$$E_d = \sqrt{\frac{\Delta\mathbf{d}^T\Delta\mathbf{d}}{N}}, \tag{9}$$

where N is the number of data. To quantify inversion results we also introduce a model error defined by

$$E_m = \sqrt{\frac{\Delta\mathbf{m}_x^T\Delta\mathbf{m}_x}{M}}, \tag{10}$$

where $\Delta\mathbf{m}_x$ indicates the difference between the inverted model and the true model, and M is the number of model parameters.

The Gauss-Newton method involves the generation of partial derivatives of forward solutions with respect to model parameters. For each frequency and source the sensitivity function $\mathbf{J}$ is a $[2\times(NG\text{-}1)]\times M$ rectangular matrix. For example, for the i-th source at a fixed frequency, the entry in the Jacobian matrix corresponding to the j-th receiver and the q-th model parameter is

$$\frac{\partial t_{ji}}{\partial m_q} = \frac{1}{p_{1i}}\left(\frac{\partial p_{ji}}{\partial m_q} - \frac{p_{ji}}{p_{1i}}\frac{\partial p_{1i}}{\partial m_q}\right), \tag{11}$$

Here, the sensitivity is a function of the partial derivatives of impulse responses which are independent of the source spectrum (see Appendix). Therefore, the full-waveform inversion of seismic data does not require the knowledge of the actual source waveform,

and this feature is the essence of the inversion algorithm using normalised wavefields (Lee and Kim, 2003).

NUMERICAL EXAMPLE

1. Model

The model used for clarifying the algorithm to be described in this paper is the same as the one in Lee and Kim (2003), a broken dipping fault in a background of 3000 m/s constant velocity as shown in Figure 1(a). The fault consists of a 6 m thick low velocity (2500 m/s) layer overlain by another 6 m thick high velocity (3500 m/s) layer. A grid set consisting of 200 by 260 elements of uniform cell size, 3 m by 3 m, has been used to compute pressure wavefields using a finite-element modelling scheme.

A crosshole configuration is used for the exercise, with the source borehole at x = - 45 m and the receiver borehole at x = 45 m. A total of 21 line sources are used with an equal vertical separation of 9 m, and the same number and separation are used for the receivers. For each source, the pressure wavefields computed at the 21 receiver positions have been normalised by the first pressure wavefield, resulting in 20 normalised wavefields.

In contrast to the time-domain inversion that theoretically requires all frequencies at once, a limited number of frequencies is sufficient for a reasonably stable and accurate inversion in the frequency domain (Pratt, 1999); too few frequency components will result in an unstable inversion or possibly a local minimum, while too many frequencies will simply increase redundancy and waste computer resources and time. We reduce the number of frequencies from ten in Lee and Kim (2003) to six: 10, 20, 40, 60, 80, and 100 Hz. Prior to inversion, 5% Gaussian noise was added to the synthetic data.

2. Weighted Regularised Inversion

In regularised inversion, we employ the Occam approach, first proposed by Constable et al. (1987) (see also deGroot-Hedlin and Constable, 1990; Parker, 1994), to determine an optimum Lagrange multiplier λ during the course of an inversion. The unique feature of the Occam approach is that the parameter λ is used in each iteration both as a step length control and a smoothing parameter. That is, the observation equation (8) is solved for a series of trial values of λ, and for each λ the misfit defined by equation (9) is evaluated by solving the forward problem, equation (1). The Occam process thus chooses a model with the minimum misfit as the basis for the next iteration. The minimisation can be carried out by a simple 1D line search.

The domain to be reconstructed is 120 m by 180 m (40 by 60 elements), containing a total of 2400 velocity parameters. The size of the matrix from equation (8) is modest for the test model, so we solve it using QR decomposition with successive Householder transformations. The data-weighting matrix $\mathbf{W}_d$ is usually a diagonal matrix, whose elements are equal to the reciprocals of data standard deviations. If we have no such information, $\mathbf{W}_d$ may be set to a diagonal matrix with its elements equal the inverse of the measurement (Torres-Verdin et al., 2000). In the first inversion exercise, we do not use model weights, i.e., $\mathbf{W}_m = \mathbf{I}$.

The first example starts with an initial guess of 2850 m/s uniform velocity. For this initial model, the inversion converges to reduce the misfit E_d from 0.297 to 0.049 after four iterations; synthetic data are successfully reproduced to a degree that is justified by the noise added. As shown in Figure 1(b), the faults are imaged correctly, but the images are smeared both vertically and horizontally, which is mainly due to the constraint of model smoothness imposed for stabilising the inversion. This result is comparable to that in Lee and Kim (2003, Figure 2(c)), who obtained their result with ten frequencies, clearly showing that there was redundancy of data. Note that not only the data misfit but also the Lagrange multiplier decreases as iteration continues, as shown in Figure 2.

In all inversion exercises except the first one, the model-weighting matrix $\mathbf{W}_m$ is derived from the sensitivities of data with respect to model parameters. An integrated sensitivity G_j for a model parameter m_j can be defined as (de Lugao et al., 1997)

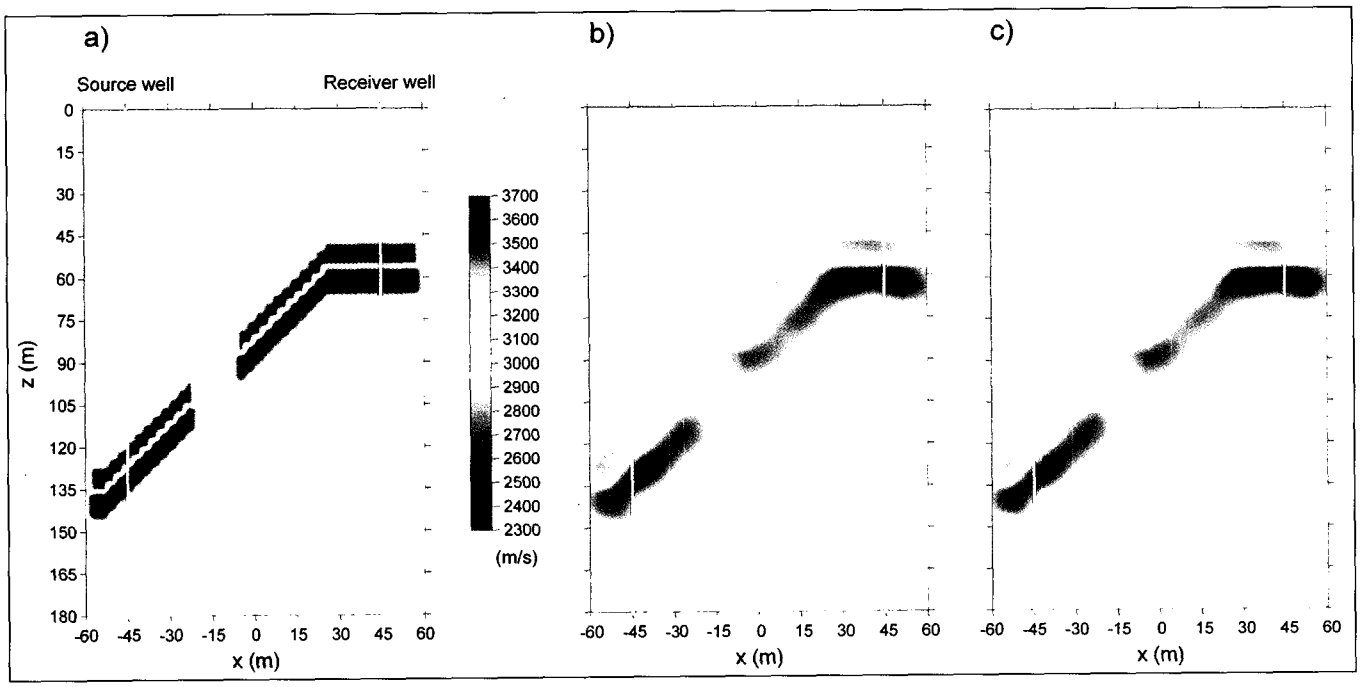

Fig. 1. Comparison of full-waveform inversion results for a fault model. Starting model used for the inversion is a 2850 m/s uniform velocity. a) A 2D velocity model. b) Inversion result without model weights. c) Inversion result with model weights.

$$G_j = \sqrt{\sum_{i=1}^{N} (J_{i,j})^2}\ , \qquad j = 1, 2, \ldots, M. \tag{12}$$

Using the integrated sensitivity, an element of $\mathbf{W}_m$ may be set to

$$W_{m,j} = \begin{cases} 1, & 0 \le \sqrt{G_j} \le c, \\ c/\sqrt{G_j}, & \sqrt{G_j} \ge c, \end{cases} \tag{13}$$

where c is a constant and set to an average value of G_j. Note that equation (13) has the same form as the Huber's M-estimator (Huber, 1964; Kim et al., 1996). Since the robust non-l_2 measure is applied to the model roughness, $\mathbf{W}_m$ plays a role of selectively making the smoothness constraint loose.

If we set $\lambda_i = \lambda W_{m,i}^2$ ($i = 1, 2, \ldots, M$) and $\varepsilon = 0$ in equation (7) or (8), then it is formally equivalent to the spatially varying Lagrange multiplier developed by Yi et al. (2001), although they derived it on the basis of the Backus-Gilbert spread function. One of the most useful advantages of using a constant Lagrange multiplier is that it can be automatically determined in the inversion from the minimum misfit criterion described above. The effect of model weights is shown in Figure 1(c), which is also obtained after four iterations to reduce its error to 0.050, almost the same level as in Figure 1(b).

Although the fault images are smeared both vertically and horizontally, mainly due to the smoothness constraint for stabilising the inversion, the smearing appears to be slightly less in Figure 1(c) than in Figure 1(b). The inversion with model weights appears to be of better quality than the inversion without them, displaying fewer artefacts especially below the faults. In fact, the final model error E_m of 101.0 in Figure 1(c) is slightly less than that of 107.0 in Figure 1(b), while both data errors are nearly the same. Note that the model error of the initial guess is 207.7.

3. Single-Frequency Inversion

The overall quality of the inversion may be improved by adopting a staged approach, inverting at single frequencies sequentially from low frequencies to high frequencies (e.g., Song et al., 1995; Pratt, 1999), instead of inverting all frequency components simultaneously. A consecutively ordered single-frequency inversion is particularly useful from the viewpoint of computation efficiency if the total number of iterations required for convergence is similar to that in the multi-frequency simultaneous inversion. The single-frequency inversion is analogous to obtaining the response of a single-frequency oscillator in the time domain. Yokota and Matsushima (2004) showed that a multi-frequency inversion can be carried out by multiple single-frequency inversions.

In single-frequency inversion, the selection of an optimal frequency is crucial for inversion efficiency and stability. Yokota and Matsushima (2004) suggested that the frequency must be determined so as to avoid cycle skipping. Figure 3 shows the set of frequencies used in this paper for multiple single-frequency inversion. The maximum wavenumber, $k_{max}(f)$, which is closely related to the minimum resolvable size of the geological structure, is given by

$$k_{max}(f) = \sqrt{\frac{4\pi f}{LV}}, \tag{14}$$

where L is the ray-path length and V is the background velocity (Williamson, 1991). Lower frequency data should be used first for stable inversion.

Figure 4 shows a velocity image reconstructed from the multiple single-frequency inversion for the fault model shown in Figure 1(a). We use the same starting model with 2850 m/s uniform velocity as in Figure 1. The inversion is terminated after six iterations as shown in Figure 5; after starting from the lowest frequency of 10 Hz, the frequency is increased for the next iteration. The convergence rate and process are, respectively, slower and more complicated than those in multiple-frequency inversion (Figure 2). The final misfit is 0.059, which is slightly higher than 0.049 (Figure 1(b)) or 0.050 (Figure 1(c)), suggesting that more inversion iterations are required to obtain a fully converged image. The quality of the inverted model is also slightly insufficient; the model error in Figure 4 is 109.6, slightly higher than 107.0 in Figure 1(b) and 101.0 in Figure 1(c).

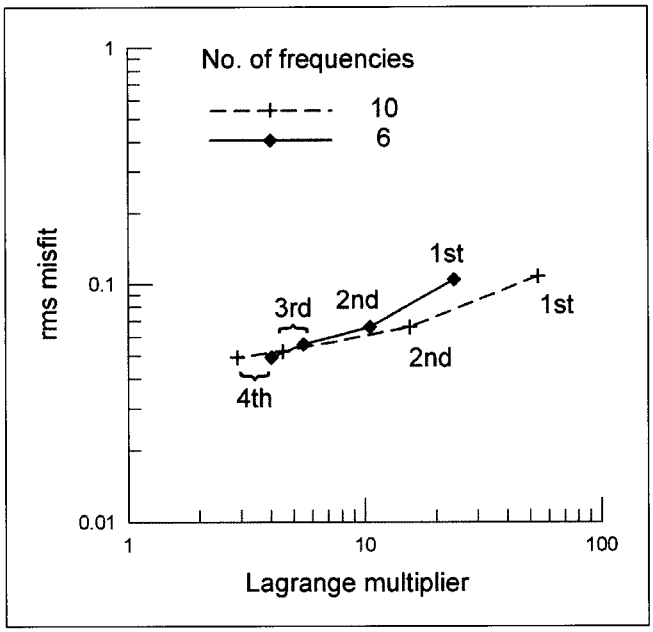

Fig. 2. Comparison of numbers of frequencies in convergence in rms misfits and the associated Lagrange multipliers, as a function of iteration, during the full-waveform inversion with a 2850 m/s uniform velocity starting model.

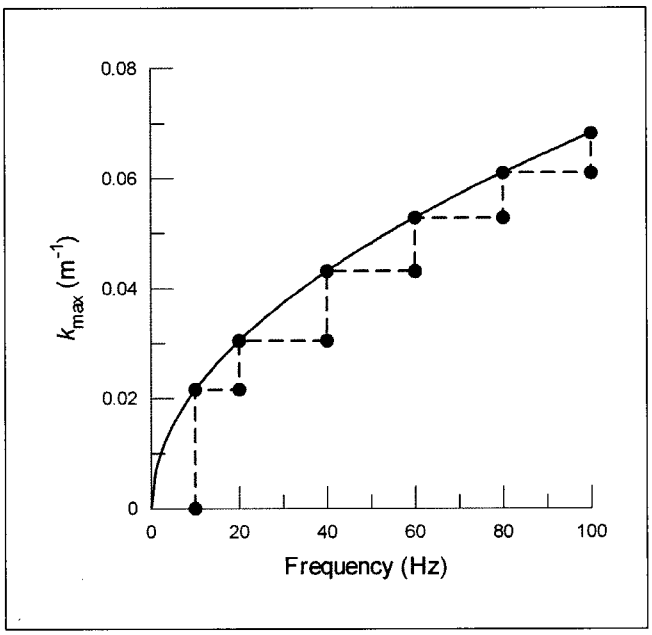

Fig. 3. A scheme for frequency selection, depending on the maximum wavenumber determined by the resolution of inversion.

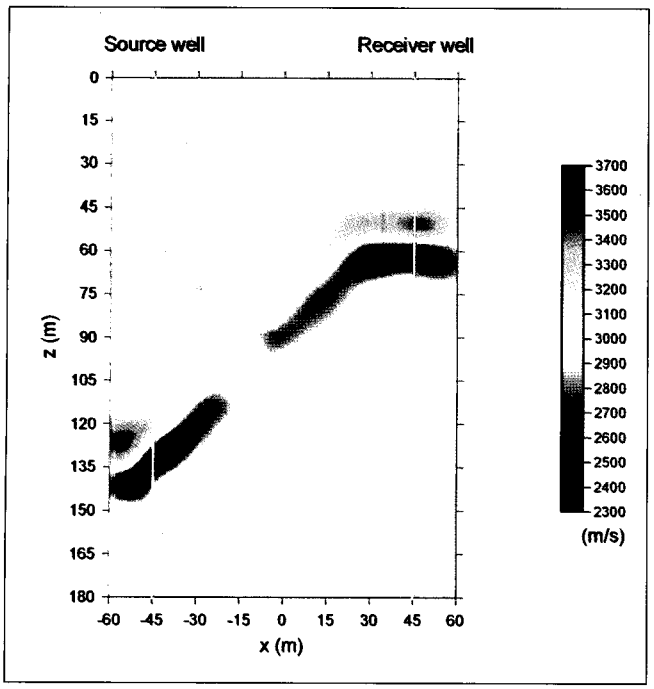

Fig. 4. Reconstructed image of multiple single-frequency inversion for the fault model shown in Figure 1(a). Starting model used for the inversion is a 2850 m/s uniform velocity.

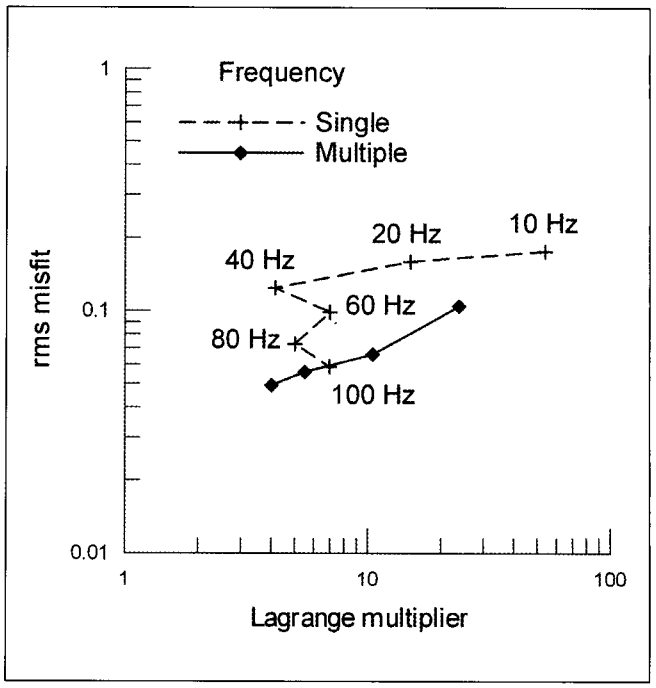

Fig. 5. Comparison of convergence of staged single-frequency inversion with multiple-frequency inversion. The figure shows rms misfits and the associated Lagrange multipliers as a function of iteration.

If two inversion iterations are made for each single-frequency step, for example, we can obtain a fully converged model (not shown) whose final misfit and model error are 0.051 and 106.5, respectively. However, such a double-loop algorithm (Yokota and Matsushima, 2004) takes twice the computation time compared with the single-loop algorithm used in Figure 4, although it is still faster than the multiple-frequency inversion method. Further research is required to determine criteria for how many iterations are optimum at each frequency, and which frequency is selected for the next iteration, in the single-frequency inversion, although these would be highly model-dependent.

CONCLUSIONS

A rigorous full-waveform inversion of seismic data has been a challenging subject partly because of the lack of precise knowledge of the source. To avoid potential inversion errors due to source estimation required in conventional full-waveform inversion methods, Lee and Kim (2003) developed a full-waveform inversion scheme using normalised wavefields. In this paper, we have modified their scheme to install a weighted smoothness constraint for better resolution and to adopt a staged approach, inverting normalised wavefields in order of frequency. The validity of the modified scheme is successfully demonstrated using a simple 2D synthetic model, which is the same one as used in Lee and Kim (2003). The inversion with model weights appears to have fewer artefacts than the inversion without them. The model weight for selectively relaxing the smoothness constraint is determined on the basis of integrated sensitivities. The multi-frequency simultaneous inversion can almost be replicated by multiple single-frequency inversions. In particular, the consecutively ordered single-frequency inversion is useful for computation efficiency. Selection of optimum frequency and extension to 3D problems with applications to real data requires further investigation.

ACKNOWLEDGMENTS

This work was supported by the Japan Society for the Promotion of Science (AP210334027) and the Korea Science and Engineering Foundation (F03-2003-000-20008-0). We thank Ki Ha Lee and the reviewers and editors for their constructive comments.

REFERENCES

Cerveny, V., and Soares, J.E.P., 1992, Fresnel volume ray tracing: *Geophysics*, **57**, 902–915.

Constable, S.C., Parker, R.L., and Constable, C.G., 1987, A practical algorithm for generating smooth models from electromagnetic sounding data: *Geophysics*, **52**, 289–300.

deGroot-Hedlin, C., and Constable, S., 1990, Occam's inversion to generate smooth, two-dimensional models from magnetotelluric data: *Geophysics*, **55**, 1613–1624.

de Lugao, P., Portniaguaine, O., and Zhdanov, M.S., 1997, Fast and stable two-dimensional inversion of magnetotelluric data: *Journal of Geomagnetism and Geoelectricity*, **49**, 1437–1454.

Frazer, L.N., Sun, X., and Wilkens, R.H., 1997, Inversion of sonic waveforms with unknown source and receiver functions: *Geophysical Journal International*, **129**, 579–586.

Frazer, L.N., and Sun, X., 1998, New objective functions for waveform inversion: *Geophysics*, **63**, 213–222.

Humphreys, E., and Clayton, R.W., 1988, Application of back-projection tomography to seismic traveltime problems: *Journal of Geophysical Research*, **93**, 1073–1085.

Huber, P.J., 1964, Robust estimation of a location parameter: *Annals of Mathematical Statistics*, **35**, 73–101.

Kim, H.J., Fujisaki, O., and Takeuchi, M., 1996, Two-dimensional resistivity inversion with robust estimation: *Butsuri-Tansa*, **49**, 110–116.

Kormendi, F., and Dietrich, M., 1991, Nonlinear waveform inversion of plane-wave seismograms in stratified elastic media: *Geophysics*, **56**, 664–674.

Lee, K.H., and Kim, H.J., 2003, Source-independent full-waveform inversion of seismic data: *Geophysics*, **68**, 2010–2015.

Lines, L.R., and Treitel, S., 1984, Tutorial: A review of least-squares inversion and its application to geophysical problems: *Geophysical Prospecting*, **32**, 159–186.

Minkoff, S.E., and Symes, W.W., 1997, Full waveform inversion of marine reflection data in the plane-wave domain: *Geophysics*, **62**, 540–553.

Nolet, G., 1985, Solving or resolving inadequate and noisy tomographic systems: *Journal of Computational Physics*, **61**, 463–482.

Parker, R.L., 1980, The inverse problem of electromagnetic induction: existence and

construction of solutions based upon incomplete data: *Journal of Geophysical Research*, **85**, 4421–4425.

Parker, R.L., 1994, *Geophysical Inverse Theory*, Princeton University Press.

Peterson, J.E., Paulson, B.N.P., and McEvilly, T.V., 1985, Applications of algebraic reconstruction techniques to crosshole seismic data: *Geophysics*, **50**, 1566–1580.

Plessix, R.-E., and Bork, J., 1998, A full waveform inversion example in VTI media: *68th Annual International Meeting, Society of Exploration Geophysicists, Expanded Abstracts*, 1562–1565.

Pratt, R.G., 1999, Seismic waveform inversion in frequency domain, Part 1: Theory and verification in physical scale model: *Geophysics*, **64**, 888–901.

Pratt, R.G., and Shipp, R.M., 1999, Seismic waveform inversion in frequency domain, Part 2: Fault delineation in sediments using crosshole data: *Geophysics*, **64**, 902–914.

Sasaki, Y., 1989, Two-dimensional joint inversion of magnetotelluric and dipole-dipole resistivity data: *Geophysics*, **54**, 254–262.

Scales, J.A., Gersztenkorn, A., and Treitel, S., 1988, Fast solution of large sparse, linear systems: Application to seismic traveltime tomography: *Journal of Computational Physics*, **75**, 314–333.

Sen, M.K., and Stoffa, P.L., 1991, Nonlinear one-dimensional seismic waveform inversion using simulated annealing: *Geophysics*, **56**, 1624–1638.

Sheng, J., and Schuster, G.T., 2000, Finite-frequency resolution limits of traveltime tomography for smoothly varying velocity models: *70th Annual International Meeting, Society of Exploration Geophysicists, Expanded Abstracts*,, 2134–2137.

Song, Z.-M., Williamson, P.R., and Pratt, R.G., 1995, Frequency-domain acoustic wave modeling and inversion of crosshole data: Part II-inversion method, synthetic experiments and real-data results: *Geophysics*, **60**, 796–809.

Tikhonov, A.N., and Arsenin, V.Y., 1977, *Solutions to Ill-Posed Problems*, John Wiley and Sons, Inc.

Torres-Verdin, C., Druskin, V.D., Fang, S., Knizhnerman, L.A., and Malinverno, A., 2000, A dual-grid nonlinear inversion technique with applications to the interpretation of dc resistivity data: *Geophysics*, **65**, 1733–1745.

Vasco, D.W., 1991, Bounding seismic velocities using a tomographic method: *Geophysics*, **56**, 472–482.

Vasco, D.W., Peterson, Jr., J.E., and Majer, E.L., 1995, Beyond ray tomography: Wavepaths and Fresnel volumes: *Geophysics*, **60**, *1790–1804*.

Williamson, P.R., 1991, A guide to the limits of resolution imposed by scattering in ray tomography: *Geophysics*, **56**, 202–207.

Yi, M.-J., Kim, J.-H., Song, Y., Cho, S.-J., Chung, S.-H., and Suh, J.-H., 2001, Three-dimensional imaging of subsurface structures using resistivity data: *Geophysical Prospecting*, **49**, 483–497.

Yokota, T., and Matsushima, J., 2004, Seismic waveform tomography in the frequency-space domain: selection of the optimal temporal frequency for inversion: *Exploration Geophysics*, **35**, 19–24.

Zhou, B., and Greenhalgh, S.A., 2003, Crosshole seismic inversion with normalized full-waveform amplitude data: *Geophysics*, **68**, *1320–1330*.

Zhou, C., Schuster, G.T., Hassanzadeh, S., and Harris, J.M, 1997, Elastic wave equation traveltime and wavefield inversion of crosswell data: *Geophysics*, **62**, 853–868.

APPENDIX: SENSITIVITY ANALYSIS

A 2D acoustic wave equation with a source term s is given by

$$\nabla^2 p + \frac{\omega^2}{v^2} p + s = 0 . \tag{A1}$$

If we assume $v = v_b + \Delta v$, where subscript b indicates the background, the generalised Green's function is given by

$$\nabla^2 g + \frac{\omega^2}{v_b^2} g + \delta = 0 . \tag{A2}$$

Let $m = 1/v^2$ ($= \rho/\lambda$, where ρ is the density and λ is the wave length), we have

$$\nabla^2 p + m\omega^2 p + s = 0 , \tag{A3}$$

$$\nabla^2 g + m_b \omega^2 g + \delta = 0 . \tag{A4}$$

Taking $\int [g \times (\mathrm{A3}) - p \times (\mathrm{A4})] dS$ and letting $\Delta m = m - m_b$ gives

$$p = p_b + \omega^2 \int g \Delta m p dS . \tag{A5}$$

The partial derivative of i-th data due to k-th source with respect to a parameter m_j at j-th element is

$$\frac{\partial p(i,k,\omega)}{\partial m_j} = \omega^2 \lim_{\Delta m_j \to 0} \left[\int_{S_j} g \Delta m p dS \Big/ \Delta m \right] . \tag{A6}$$

Since $g \to p$ when $\Delta m_j \to 0$, equation (A6) can be rewritten as

$$\frac{\partial p(i,k,\omega)}{\partial m_j} = \omega^2 \int_{S_j} p(i,j,\omega) p(j,k,\omega) dS , \tag{A7}$$

or from reciprocity

$$\frac{\partial p(i,k,\omega)}{\partial m_j} = \omega^2 \int_{S_j} p(j,i,\omega) p(j,k,\omega) dS . \tag{A8}$$

Consequently, we have

$$\frac{\partial p(i,k,\omega)}{\partial v_j} = -\frac{2\omega^2}{v_j^3} \int_{S_j} p(j,i,\omega) p(j,k,\omega) dS . \tag{A9}$$

정규화된 탄성파 파동장 자료의 향상된 전파형 역산

김희준[1], Toshifumi Matsuoka[2]

요 약: 정규화된 파동장을 이용하는 탄성파 전파형 역산법은 기존의 전파형 역산법에서 필요로 하는 탄성파원 예측으로 인해 야기되는 잠재적인 역산오차를 피할 수 있다. 본 논문에서는 이러한 전파형 역산법에 가중 평활화제약을 추가하여 분해능을 높였으며, 모든 주파수성분을 동시에 역산하지 않고 주파수 별로 순차적으로 역산하도록 수정하였다. 새로운 방법은 간단한 2 차원 단층모델에 적용하여 검증하였다. 가장 큰 개선점은 적분감도에 기초하여 결정한 가중계수를 모델변수에 도입한 점이다. 모델변수에 가중계수를 적용하면 평활화제약을 선택적으로 완화할 수 있기 때문에 영상화 재구성 시 잘못된 영상을 줄이는데 효과적이다. 다중 단일주파수 역산은 다중주파수 동시역산을 대치할 수 있으며, 특히 작은 주파수부터 먼저 사용하는 순차적인 단일주파수 역산은 계산효율면에서 유용하다.

주요어 : 시추공간 탐사, 전파형, 토모그래피, 정규화된 파동장, 감도

正規化された地震波動場データのフルウエーブインバージョンの改良

金 喜俊（キム・ヒジュン）[1]・松岡俊文[2]

要 旨: 正規化された波動場を用いるサイスミックフルウエーブインバージョン法は、既存の方法で必要とされる波源の推定に伴う潜在的な誤差を避けることが出来る。本報ではこのようなフルウエーブインバージョン法における分解能の向上を目指して、重み付き平滑化制約を追加し、また全ての周波数成分を同時にインバージョンするのではなく、各週波数成分を順次インバージョンすることにした。この新しい方法は簡単な２次元断層モデルに適用して検証した。最も改善された点は、積分感度に基づいて決められた重み係数をモデルパラメータに導入したことである。これにより、モデルパラメータにかかる平滑化制約を選択的にゆるめることが出来るので、イメージを再構成する際に生じる偽のイメージを抑えるのに効果的である。単一周波数成分の段階的インバージョンは、多重周波数同時インバージョンに取って替わることが可能であり、特に低い周波数から順に使用する単一周波数インバージョンは計算効率の面で有利である。

キーワード：坑井間、フルウェーブ、トモグラフィ、正規化された波動場、感度

1 부경대학교, 환경탐사공학과
608-737 부산시 남구 대연동 559-1,
2 교토대학대학원공학연구과 사회기반공학전공

1 釜慶大学校環境海洋大学 地球環境科学群環境探査工学科
2 京都大学工学研究科 社会基盤工学専攻工学専攻